THE JOURNAL OF PHYSICAL CHEMISTRY C

Article

pubs.acs.org/JPCC

Growth Mode Transition from Monolayer by Monolayer to Bilayer by Bilayer in Molecularly Flat Titanyl Phthalocyanine Film

Jun Hong Park,[†] Lalitasri Ravavar,[§] Iljo Kwak,[†] Susan K. Fullerton-Shirey,[∥] Pabitra Choudhury,[§] and Andrew C. Kummel*[,†,‡]

[†]Materials Science & Engineering Program, University of California, San Diego, La Jolla, California 92093, United States

[‡]Departments of Chemistry & Biochemistry, University of California, San Diego, La Jolla, California 92093, United States

[§]Department of Chemical Engineering, New Mexico Tech, Socorro, New Mexico 87801, United States

[∥]Department of Chemical and Petroleum Engineering, University of Pittsburgh, Pittsburgh, Pennsylvania 15213, United States

Supporting Information

ABSTRACT: To avoid defects associated with inhomogeneous crystallites and uneven morphology that degrade organic device performance, the deposition of ultraflat and homogeneous crystalline organic active layers is required. The growth mode transition of organic semiconducting titanyl phthalocyanine (TiOPc) molecule from monolayer-by-monolayer to bilayer-by-bilayer can be observed on highly ordered pyrolytic graphic (HOPG), while maintaining large and molecularly flat domains. The first monolayer of TiOPc lies flat on HOPG with a ∼98% face-up orientation. However, as the thickness of the TiOPc increases to over 15 monolayers (ML), the growth mode transitions to bilayer-by-bilayer with the repeated stacking of bilayers (BL), each of which has face-to-face pairs. Density functional theory calculations reveal that the increasing of thickness induces weakening of the substrate effect on the deposited TiOPc layers, resulting in the growth mode transition to BL-by-BL. The asymmetric stacking provides the driving force to maintain nearly constant surface order during growth, allowing precise, subnanometer thickness control and large domain growth.

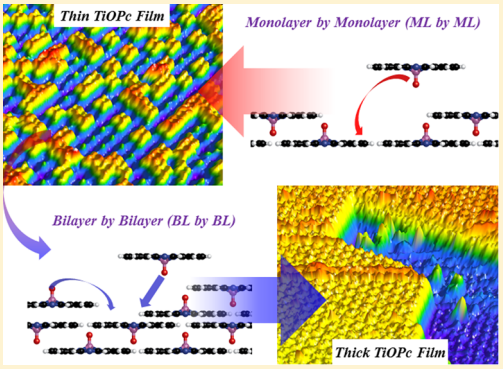

INTRODUCTION

Although inorganic Si and III-V materials have led the modern semiconductor industry for half a century, the integration of organic thin films has been expanded to microelectronics for displays, solar cells, and platforms for electronic skins.[1−8] These organic thin film transistors (OTFT) and organic photovoltaics (OPV) provide low cost, mechanical flexibility, and direct bandgap modulation for electroluminescence. In flexible organic electronics, molecular orientation, degree of crystallinity, and morphology govern carrier transport and injection between organic layers and electrodes;[9−14] therefore, the development of homogeneous crystalline organic channels on flexible electrodes is crucial. Taking advantage of its high strength and enhanced photovoltaic efficiency during deformation, graphene has recently been employed as a flexible electrode for OTFTs and OPV.[15−17] Therefore, to fabricate flexible organic devices integrated onto graphene electrodes, it is essential to deposit organic layers on graphene, while maintaining the growth of ultraflat large domains. Moreover, the growth of organic layers with nearly atomic flat surfaces and large domain sizes is not only required to template uniform deposition of organic heterostructures but may also enable bandgap engineering of the contacts.

The growth of aromatic organic films relies on van der Waals interactions between organic molecules.[18−20] During the deposition of organic layers, the growth of the films can involve directional molecular packing, resulting from the shape anisotropy of molecules. In many cases, the molecule−substrate interaction is stronger than molecule−molecule interaction; therefore, the molecules form a flat monolayer on substrates in the initial growth stage.[20−22] However, upon additional organic molecular deposition, the molecule−substrate interaction can be overwhelmed by molecule−molecule interactions, resulting in a new molecule−substrate geometry such as "standing" molecular orientation.[20−24] Moreover, because the multilayer growth of organic molecules mostly involves step flow, island, or layer-plus-island growth modes during the deposition,[19−28] it is hard to simultaneously obtain precise thickness control, ultraflat topology, and large domain growth. These orientation transitions and absence of layer-by-layer growth normally result in inhomogeneous crystallites that induce charge trapping at interfaces in OTFT or unintentional recombination of excitons at defects states in OPV.[29,30]

Received: December 30, 2016
Revised: March 5, 2017
Published: March 7, 2017

DOI: 10.1021/acs.jpcc.6b13096
J. Phys. Chem. C 2017, 121, 6721−6728

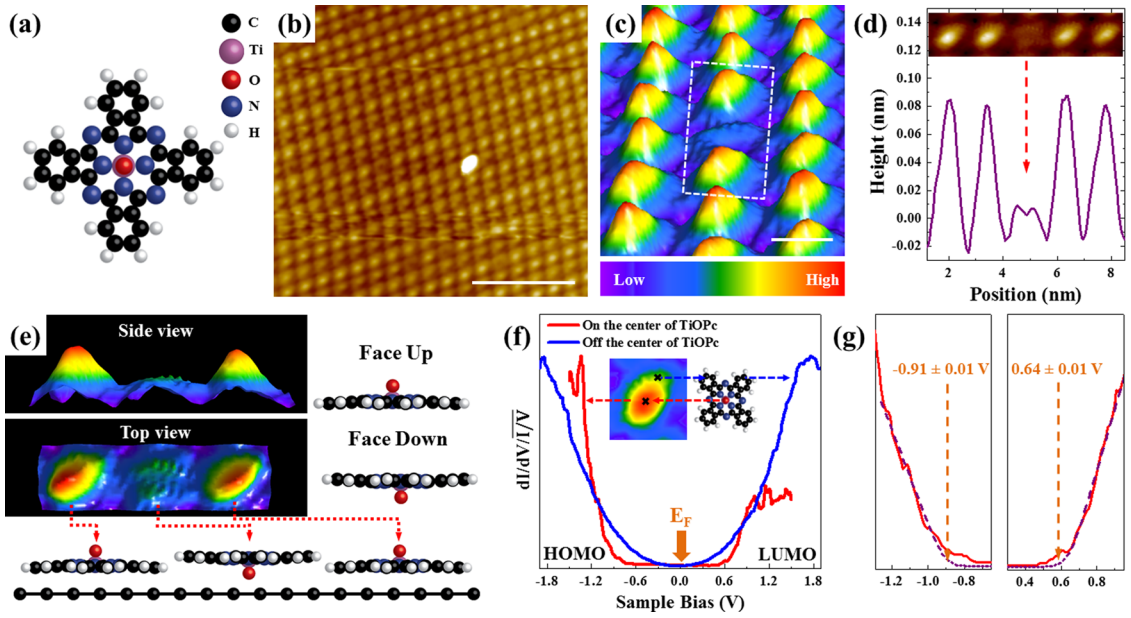

Figure 1. Empty state STM images and STS of monolayer TiOPc on HOPG. STM images recorded with Vs = +2.0 V, It = 20 pA at 100 K. (a) Molecular structure of TiOPc. (b) 1 ML TiOPc deposited by MBE on HOPG at 373 K. Scale bar = 10 nm. (c) 3D rendered molecular-resolution STM image of ML. Both face up (majority) and down (minority) oriented molecules are shown. Scale bar = 1 nm. (d) Line trace of both face up and down oriented moelcules. (e) Schematic diagram of TiOPc ML based on the STM image. (f) $(dI/dV)/(I/V)$ data from TiOPc ML on HOPG. The locations of the STS measurements are marked as × in the superimposed STM image. (g) Expanded STS from −1.3 to −0.7 V and 0.3 to 0.9 V where the onset of differential current occurs; spectra taken at the center of the TiOPc.

In this report, the quasi-2D (two-dimensional) growth of titanyl phthalocyanine (TiOPc) multilayers deposited on graphite is observed via scanning tunneling microscopy (STM). Multiple metal phthalocyanines have been studied as hole transport layers in organic light-emitting diodes (OLED),[31,32] dyes, catalysts, coating for DC ROMs,[33] donor materials in OPV,[2,34] and active layers for chemical sensing.[35,36] In particular, TiOPc has been employed for organic photovoltaic cells, due to its broad photoelectrical activity from the visible to the near IR.[2,37,38] The growth of TiOPc is dominated by its polarity and shape; since TiOPc has an O atom on top of the central Ti, it has a dipole and a nonplanar shape similar to other metal oxide phthalocyanine such as vanadyl phthalocyanine.[39] Therefore, the growth behavior of TiOPc is very different from planar molecules but likely similar to other nonplanar, polar, aromatic metal coordination complexes.[40−42] Previously, the stacking configurations of nonplanar shaped TiOPc and SnPc (tin(II)-phthalocyanin) in ultrathin layers (less than four monolayers) were reported on Ag(111) and 3,4,9,10-perylenetetracarboxylic dianhydride (PTCDA) functionalized Ag(111).[40,43] It also was reported that the TiOPc layers are grown via "bilayer by bilayer" mode on Ag(111) using ultraviolet photoelectron spectroscopy (UPS), after deposition of 4 ML (monolayer). Conversely, in this report, the highly oriented pyrolytic graphite (HOPG) is employed as a substrate and the growth behavior is studied for thick layers (about 5−10 nm), which are close to actual active layer thicknesses in OTFT. The multiple ring structure in TiOPc along with the molecular dipole[44] and asymmetric shape induce layer-by-layer growth of thin multilayers with a negligible increase in roughness and large domains on each HOPG terrace. However, for thick multilayers, a transition is observed from monolayer-by-monolayer (ML-by-ML) growth to bilayer-by-bilayer (BL-by-BL) growth, and this growth mode transition occurs at greater thickness on HOPG than on Ag(111).[41,44,45] Although the transition from ML-by-ML to BL-by-BL growth has been previously reported for 4 ML TiOPc/Ag(111),[43] the growth mode transition to BL-by-BL on HOPG is induced at greater layer thickness (15 ML); the difference may be consistent with the greater screening of the TiOPc dipole for the oriented TiOPc layers by Ag(111) than HOPG. The deposition on HOPG allows experimental determination of the electronic structure as a function of film thickness via scanning tunneling spectroscopy with minimal influence of the substrate and facile Density functional theory (DFT) modeling of the mechanism for ML-by-ML since the HOPG surface can readily by modeled by a single layer.

EXPERIMENTAL SECTION

Highly oriented pyrolytic graphite (HOPG) samples were cleaved freshly in air by mechanical exfoliation, then transferred into the UHV chamber immediately. After transferring the HOPG into the UHV chamber, samples were annealed at 750 K to remove tape residue and air induced adsorbates. The TiOPc powder (Sigma-Aldrich) was purified by multiple sublimations with a differentially pumped effusion cell (Eberl MBE- Komponenten) in the UHV chamber. Each TiOPc monolayer was prepared by depositing thick-overlayers on clean HOPG at 473 K surface temperature by organic molecular beam epitaxy. Subsequently, the multilayer was heated to 523 K for 6 min, and a flat-lying TiOPc monolayer was formed. Formation of a monolayer was confirmed by STM imaging. Afterward, the TiOPc multilayer was deposited with 1 nm/min deposition rate onto the TiOPc monolayer at 373 K, which acts as a seeding layer. STM and STS were performed at 100 K with Omicron VT STM with etched tungsten tips. Density functional theory (DFT) calculations also were performed employing the Vienna ab initio Simulation Package (VASP), and details are included in the Supporting Information.

DOI: 10.1021/acs.jpcc.6b13096
J. Phys. Chem. C 2017, 121, 6721−6728

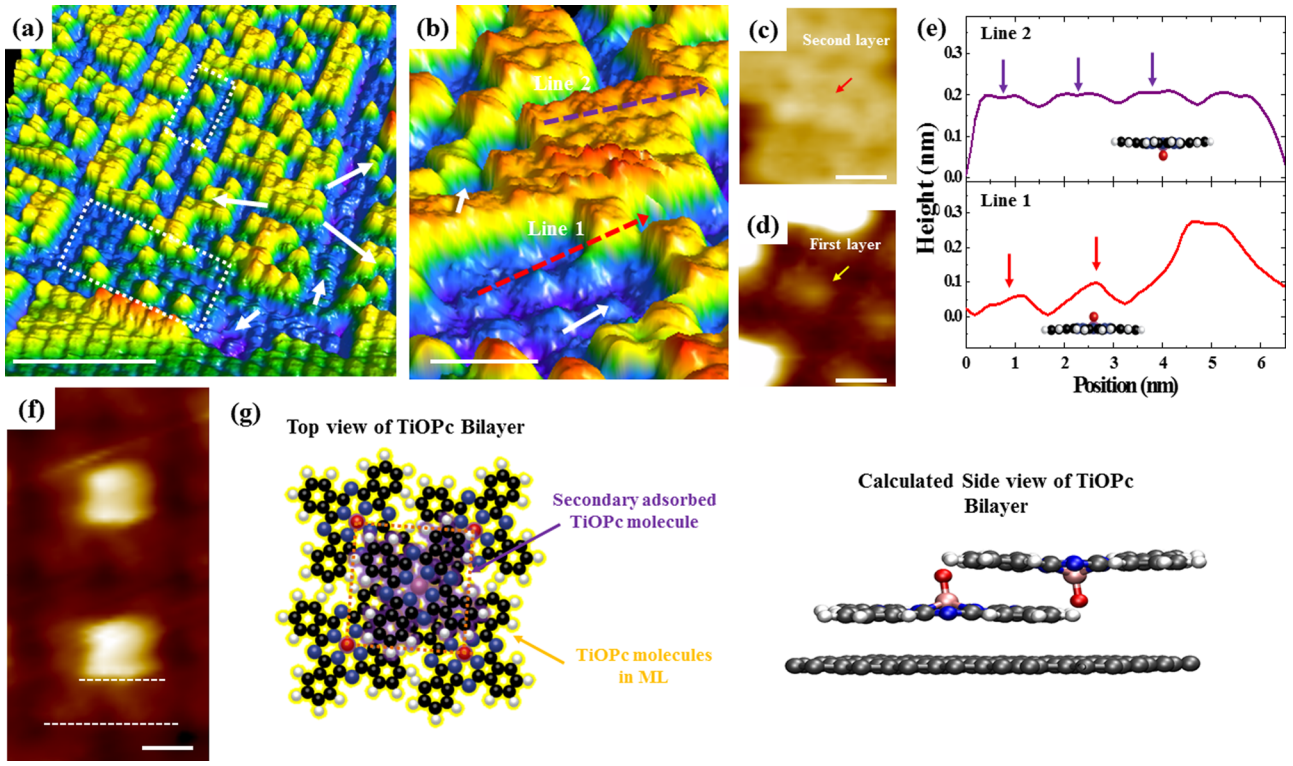

Figure 2. Empty state STM images of TiOPc bilayer on HOPG. All STM images recorded at 100 K. (a) 3D rendered STM image of a partial TiOPc bilayer (Vs = +2.0 V, It = 20 pA). Examples of single layer TiOPc are in white boxes. Scale bar = 10 nm. (b) 3D rendered STM image of a partial TiOPc bilayer (Vs = +2.0 V, It = 40 pA). Scale bar = 5 nm. (c) High-resolution STM image of a TiOPc molecule in a bilayer (second layer) (Vs = +1.5 V, It = 80 pA). (d) High-resolution STM image of a TiOPc molecule in a monolayer (first layer) (Vs = +1.5 V, It = 80 pA). (e) Line trace analysis from part b. Line 1 corresponds to the first and second layers, while line 2 corresponds to the second layer. (f) High-resolution STM image of single TiOPc molecules adsorbed on the TiOPc monolayer. Scale bar = 1 nm. (g) Stacking configuration with face up and down molecules.

RESULTS AND DISCUSSION

A flat-lying TiOPc monolayer was deposited by molecular beam epitaxy (MBE) on highly ordered pyrolytic graphite (HOPG) with a high degree of 2D crystallinity, as shown in STM images of Figure 1. Figure 1a displays the molecular structure of TiOPc; the oxygen atom is located on the central Ti, consistent with a permanent dipole from the bonding of O to Ti.[42,44] As shown in Figure 1b, empty state STM images show a defect-free monolayer (ML) of TiOPc deposited on HOPG. It is noted that the STM image in part b is distorted due to thermal drift.

A three-dimensional (3D), high-resolution STM image shows two different adsorption configurations in the ML with 1.6 ± 0.02 nm spacing, as shown in Figure 1c. Most of the TiOPc molecules possess a bright spot at the center of each TiOPc, while a few TiOPc molecules show dark holes in their centers, as shown in the white box. In empty-state images, the line trace of Figure 1c shows that the dark hole at the center of the TiOPc is about 0.08 nm lower than the bright protrusions of neighboring TiOPc molecules. From quantification of five different STM images, the bright centered TiOPc molecules have a 98% population density, while the dark centered TiOPc molecules have less than 2% population density even after annealing at 537 K. As shown by previously published UPS and penning ionization electron spectroscopy of TiOPc layers on HOPG, TiOPc molecules mostly adsorb on HOPG with the titanyl group (O-Ti group) pointing to vacuum (pointing away from HOPG surface).[41,44,45] Therefore, TiOPc molecules possessing bright centers are assigned to the face up orientated adsorption, while TiOPc molecules with the dark hole are assigned to the face down oriented adsorption, as shown in Figure 1e. It is noted that the origin of this existence of the rare face down oriented molecules in ML is unclear but may be related to the limited annealing time or substrate defects.

Scanning tunneling spectroscopy (STS) measurements in Figure 1f show two different types of density of states (DOS) depending on the position of the tip on single face-up TiOPc molecules. The DOS obtained at the ring of TiOPc has large band edge states, while the DOS of the center of TiOPc has much smaller band edge states. As shown in Figure 1g, the STS range of −1.3 to −0.7 V and 0.3 to 0.9 V from the center of TiOPc are expanded to show the onset bias at the highest occupied molecular orbital (HOMO) and the lowest unoccupied molecular orbital (LUMO). To extract the position of onset bias from measured $(dI/dV)/(I/V)$, STS modeling was employed as shown by the dashed lines; the detailed method is described in previous STM/STS studies.[46,47] Note the standard error is obtained by the fitting process in STS. The given uncertainties provided by the present fitting employing least-squares fitting are statistical, are less than thermal broadening, and do not account for band edge states.[48] The onset of the HOMO occurs at −0.91 ± 0.01 V, while the onset of the LUMO occurs at 0.64 ± 0.01 V. Therefore, although the Fermi level of the center of TiOPc is still in the band gap, it is within ~0.27 V of the LUMO. It can be hypothesized that the Fermi level being closer to the LUMO can result from the localized dipole moment at center of the TiOPc molecules, which has been confirmed in previous experimental and DFT calculation data.[41,42,44] It is noted that because of the existence of large

DOI: 10.1021/acs.jpcc.6b13096
J. Phys. Chem. C 2017, 121, 6721−6728

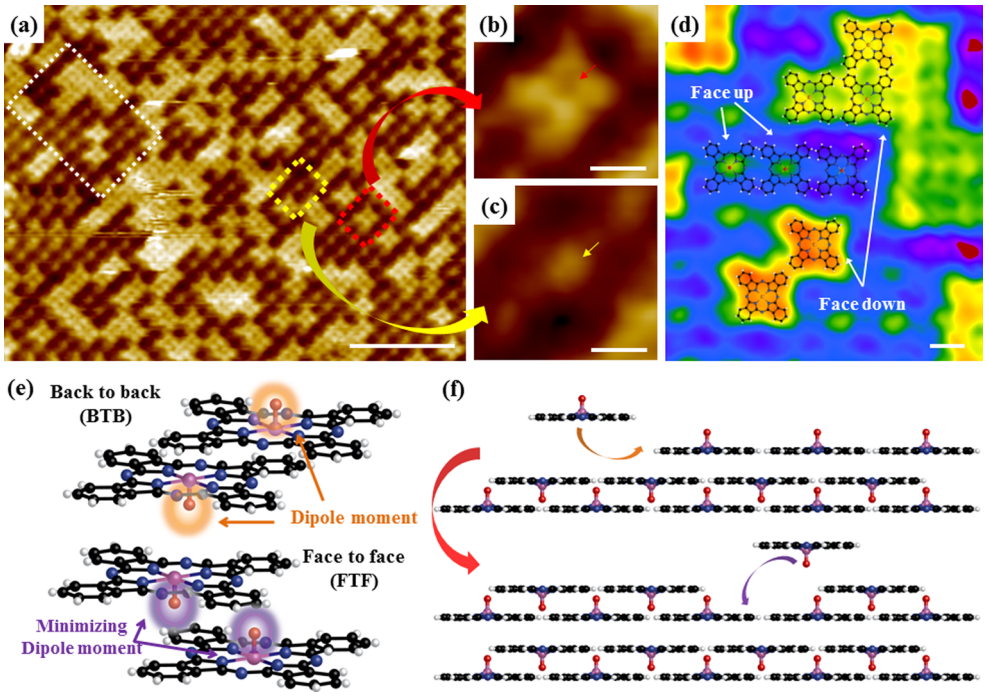

Figure 3. Empty state STM images of a thin TiOPc multilayer (about 3 nm thickness) and schematic stacking model. (a) STM image of the TiOPc multilayer (Vs = +2.0 V, It = 20 pA); the corresponding thickness is estimated as ~3 nm. Scale bar = 10 nm. (b) High-resolution STM image of a face down molecule in the top layer (Vs = +1.5 V, It = 100 pA). Scale bar = 1 nm. (c) High-resolution STM image of a face down molecule in the bottom layer (Vs = +1.5 V, It = 100 pA). Scale bar = 1 nm. (d) Molecularly resolved STM image shows face up (bottom layer) and down oriented TiOPc molecules (top layer) from a region marked by a white rectangle in part a (Vs = +2.0 V, It = 40 pA). Scale bar = 1 nm. (e) Back to back and face to face pairs in the TiOPc layer. (f) Schematic of TiOPc multilayer grown via a two-dimensional molecular layer by layer growth.

band edge states in the ring of TiOPc, it is hard to define the exact position of the onset bias in STS of the TiOPc rings.

After the deposition of additional TiOPc molecules onto the ML, flat-lying bilayer growth and island formation are observed resulting from "ML-by-ML" growth as shown in Figure 2. In Figure 2a, a 3D-rendered STM image shows BL growth on the TiOPc ML with a molecular ML-by-ML growth mode; after completion for the bottom face-up layer, each impinging molecule forms a new single molecule second-layer island or attaches to an existing island, instead of diffusing to a step edge or starting third layer growth. The existence of these single molecular islands on the first layer indicates the surface diffusion is limited and there is no step flow growth.

In the 3D rendered expanded STM image of Figure 2b and molecularly resolved STM images of Figure 2c,d, the orientation contrast between first and second layer molecules is readily observed. In BL, the slightly dark depression can be observed at the center of the molecule as shown in Figure 2c. Conversely, in ML, the bright protrusion is observed at the center of the molecule as shown in Figure 2c, consistent with opposite orientation to the TiOPc in BL. As previously stated in the discussion of Figure 1, the observation of dark holes at the center of molecules can be assigned the face down orientation of TiOPc, while the observation of a bright protrusion at the center can be assigned to the face up orientation. To confirm this contrast of adsorption configuration of molecules in the ML and BL, two line traces are obtained from the first and second layer from Figure 2b, shown as red and purple arrows, respectively, in Figure 2e. The central atoms appear as bright spots in the first layer of TiOPc molecules, suggesting the face-up orientation of nearly all TiOPc molecules as indicated by the molecular structure superimposed on Figure 2e. Conversely, the central atoms appear as dark holes in the second layer molecules, consistent with the face-down orientation of TiOPc. This growth behavior does not appear in the growth of planar CuPc molecules, as shown Figures S1–S3.

In order to elucidate the stacking configuration of the TiOPc BL, high-resolution STM is performed, as shown Figure 2f. The TiOPc molecules in the second layer in Figure 2f are observed nearly at the center of four TiOPc molecules in the first layer. As shown by the two white lines at layers 1 and 2, TiOPc molecules in layer 2 are nearly parallel to TiOPc molecules in layer 1. On the basis of the STM image and the line trace, the stacking of second layer molecules is shown in the schematic diagram on the left of Figure 2g. Assuming the central O of TiOPc is a vertex in the first layer (which is an approximation), the square unit cell, indicated by the dashed, red box, is obtained by drawing lines along four neighboring TiOPc molecules. On the basis of this unit cell, the second layer TiOPc molecule is positioned near the center of the first layer square unit cell. This binding configuration of TiOPc molecules in BL is consistent with previously published STM results of TiOPc layers on Ag(111) surfaces.[43] The pointing by O–Ti in layer 1 to the outer ring of TiOPc molecules in layer 2 is consistent with minimization of the net dipole moments of TiOPc molecules in adjacent layers, as shown in the schematic calculated by DFT of Figure 2g.

Growth behavior identical to the BLs can be observed in the thin (~2–3 nm), multilayer growth of TiOPc. It is noted that the thickness of the multilayer is estimated by quantification of pinholes in the TiOPc layer, as shown in Figure S4. Since deposition of TiOPc on HOPG for 1 min corresponds to 3–4 ML (about 1 nm thickness), it can be estimated that deposition

DOI: 10.1021/acs.jpcc.6b13096
J. Phys. Chem. C 2017, 121, 6721–6728

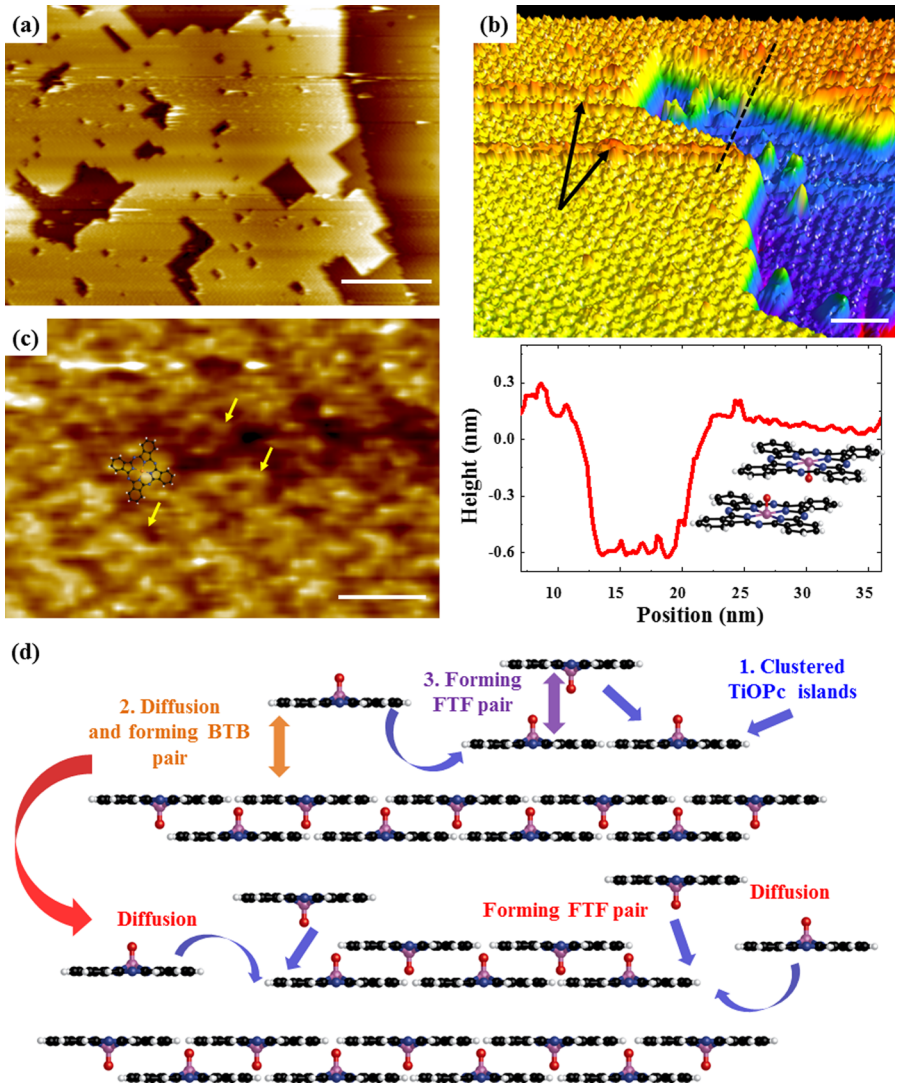

Figure 4. Empty state STM images of a thick TiOPc multilayer on HOPG. STM images recorded at 100 K (Vs = +2.0 V, It = 20 pA). (a) STM image of a thick TiOPc multilayer deposited for 5 min on a TiOPc ML at 373 K (about 5 nm thickness). Scale bar = 50 nm. (b) 3D rendered STM image showing topmost layer and corresponding line trace. Scale bar = 5 nm. (c) High-resolution STM image of the topmost layer. Yellow arrows indicate central dark hole of TiOPc. Scale bar = 2 nm. (d) Schematic model of thick TiOPc multilayer with bilayer growth mode.

for 3 min results in deposition of 9−10 ML (about 3 nm thickness). Similar with the BL, Figure 3a shows the topmost layer is grown with a ML-by-ML mode, forming a 4-fold symmetric lattice structure. As shown in Figure S6, the STM image (250 nm × 250 nm) displays that the most of molecules in topmost layer possesses nearly identical orientation, consistent with formation of larger domains. In the molecularly resolved image of Figure 3b,c, the topmost molecules appear with dark holes at the centers consistent with face down orientation, while the underneath layer shows bright centers consistent with face up orientation, as shown by the red and the yellow arrows, respectively. It is proposed that most of the topmost TiOPc are in the face down orientation, indicating stable stacking as shown in Figure 3c with the superimposed molecular structure. Therefore, the growth of face up oriented layers is not initiated until completion of the underneath layer with face down TiOPc molecules. The filling process in the face down oriented layer is shown by STM in Figure S5. It is hypothesized that during the formation of face-up oriented layers on face-down oriented layers, the diffusion speed of TiOPc molecules in the face-up layer is very fast, as shown by the formation of large face-up domains in contrast the small face-down islands.

It is noted that TiOPc layers deposited on Ag(111) have ML by ML growth only for the first 4MLs on Ag(111), and the growth mode transition to BL-by-BL growth is induced after deposition of 4 ML, confirmed by UPS.[43] However, as shown in present STM results, the ML-by-ML growth behavior on HOPG still persists ML-by-ML, even after deposition of 9−10 ML, as shown in Figure 3c. The different transition thickness may be a result of differences in screening strength of the substrates to the dipoles of TiOPc.[43]

The permanent dipole and asymmetric shape of TiOPc lead not only to molecular layer-by-layer growth in the thin multilayer but also termination by face-down molecular orientation in the BL and multilayers.[44,45] In multilayer TiOPc, two distinct molecular orientations exist depending on the direction of the protruding central O−Ti group: "back-to-back (BTB) pair" and "face-to-face (FTF) pair" orientations, as shown in Figure 3e.[42] In the BTB pair, the protruding O-Ti group faces outward, while the benzene rings of the two molecules face each other with strong $\pi-\pi$ interaction.

DOI: 10.1021/acs.jpcc.6b13096
J. Phys. Chem. C 2017, 121, 6721−6728

Conversely, the FTF pair involves TiOPc molecules with the protruding of O-Ti groups facing a benzene ring of another TiOPc, and benzene rings are faced outward. Since each TiOPc molecule has local dipole moments at its center, the O-Ti group in each layer is pointed to outer ring in a TiOPc of the adjacent layer in FTF pairs, consistent with minimizing the net electric dipole interaction between layers 1 and 2.[42,44] Therefore, the multilayers are grown by repeating BTB and FTF pairs, as shown in Figure 3f. Because the O-Ti groups of TiOPc face toward each other in FTF pairs, this configuration can have favorable dipole−dipole interactions that minimize the net dipole.[42−44]

DFT calculations elucidate the difference in bonding strengths between the BTB and FTF pairs. The favorable alignment of the dipole moments in the FTF pair is consistent with in a stronger DFT calculated interaction (1.45 eV) compared to the BTB pair (1.20 eV). It is noted that the bonding energies of the FTF and BTB pairs are calculated in the gas phase; both bonding energies on the surface of graphite or graphene differ slightly, as shown below. In summary, during the deposition of TiOPc multilayers, once TiOPc molecules form the FTF orientation, the position of the TiOPc molecules are locked due to maximizing the dipoles attractive interactions and the $\pi-\pi$ interactions in the thin film while minimizing steric repulsion. The locking of the TiOPc molecules suppresses surface diffusion, resulting in ML-by-ML growth instead of step-flow growth.

Although this layer-by-layer growth mode persists with increasing TiOPc multilayer thickness, the growth behavior transitions from ML growth to BL growth for thick films, as shown in Figure 4a. When a TiOPc multilayer is deposited over 5 min at 373 K, only a large, topmost layer is observed as shown by the STM image in Figure 4a. In the top layer, although square shaped vacancies are observed, they can be fully filled by further deposition of TiOPc molecules. The height of this topmost layer is 0.70 ± 0.02 nm as shown in Figure 4b, consistent with BL growth. It is noted that during STM imaging, the instability of STM tip was induced by the height difference between topmost layer and underneath layer and TiOPc adsorbates on the topmost layer, resulting in the observation of noise, as shown black arrows in Figure 4b. Although low tunneling conductivity in thick multilayers results in noisy STM images, a molecularly resolved STM image in Figure 4c displays each TiOPc molecules possessing a dark hole at the center, which is assigned to the Ti atoms in face-down TiOPc. Therefore, it can be concluded as the TiOPc film becomes thicker, the growth mode transitions to BL-by-BL growth, forming FTF pairs in thick multilayers. This growth mode transition from ML-by-ML to BL-by-BL can be suppressed by decreasing the deposition temperature, as shown in Figure S8.

On the basis of the molecular observations from STM imaging, the BL growth behavior is described schematically in Figure 4c. Initially, few TiOPc molecules arrive and form face up oriented clustered islands on the thick TiOPc layer, thereby forming BTB pairs with underneath face-down oriented TiOPc molecules. Afterward, face-up oriented TiOPc molecules act as nucleation seeds. TiOPc molecules adsorb on face-up oriented molecules to create FTF pairs. By repeated creation of FTF pairs and formation of face-up oriented islands, uniformly thick layers are deposited by epitaxial BL growth. The DFT calculation shows that the FTF bonding is stronger than BTB bonding, consistent with diffusion of TiOPc molecules to form FTF pairs. Because of the unique BL-by-BL growth mode of TiOPc molecules, molecularly flat, thick TiOPc multilayers are observed on graphite surfaces, forming near homogeneous crystalline layers spontaneously on each HOPG step, as shown in the large area atomic force microscopy (AFM) image of Figure S9. In the AFM images, the TiOPc film with 10 nm thickness is displayed; the uniform TiOPc layer is deposited with near single domain on each graphite steps, and distinct domain boundaries are not observed, consistent with the growth of large domains. Conversely, the growth mode of other organic molecules, such as pentacene or perylene tetracarboxylic dianhydride (PTCDA), transitions to multiple island formation in thick film, resulting in the polycrystalline films.[19,25−28,49−51]

In order to elucidate the mechanism for the growth mode transition from ML to BL growth, the bonding energies of adsorbed TiOPc molecules are calculated by density of function theory (DFT), as shown in Figure 5. Note here graphene is

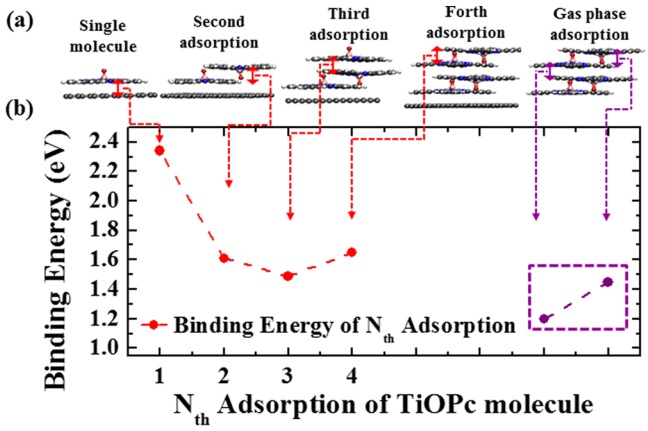

Figure 5. Calculated bonding energy of N_{th} adsorbed TiOPc molecules by density functional theory. (a) Bonding configurations of TiOPc molecules in ML, BL, and multilayer, including gas phase adsorption. (b) Bonding energy between N_{th} adsorbed TiOPc molecule and N-1_{th} adsorbed TiOPc molecule. For gas phase adsorption, two values are provided.

used as a model for the HOPG surface. Calculated bonding energies between the N_{th} TiOPc molecule and the N-1_{th} molecules on graphene are shown in Figure 5a, including the BTB and FTF pairs of TiOPc in the gas phase. In Figure 5b, a face-up oriented first layer TiOPc molecule has the highest bonding energy (2.34 eV) with the graphene substrate. Afterward, the bonding energy of face-down oriented second layer adsorbed TiOPc with first layer face-up oriented TiOPc (FTF pair) decreases to 1.61 eV. As BTB pairs are formed by the adsorption of the face-up oriented third layer molecule to a face-down oriented second layer molecule, the bonding energy decreases to 1.49 eV. However, the bonding energy of FTF pair formed between a face-down oriented forth layer TiOPc and face-up oriented third layer TiOPc increases to 1.65 eV. The increase of bonding energy in FTF pair results from favorable orientation of opposing intrinsic dipole moments and minimization of steric hindrance while maximizing $\pi-\pi$ interaction.[44] Therefore, the growth mode transition from ML growth to BL growth is consistent with the strong influence of the pre-existing TiOPc layer on the stacking of TiOPc molecules.[52] As the molecule−substrate interaction becomes weak during the growth of thick layers, the molecule−molecule

DOI: 10.1021/acs.jpcc.6b13096
J. Phys. Chem. C 2017, 121, 6721−6728

interaction dominants growth behavior, rather than molecule–substrate, resulting in a decrease of the intermolecular distance, as shown in Figure S10. In the thin multilayers, although the BTB pair has lower bonding energy than the FTF pair, formation of the FTF pairs is not initiated until full filling of the BTB pair layer, due to the substrate effect, as shown in the Supporting Information. However, because the substrate effect on the topmost layer is weak or eliminated by screening of predeposited layers in the thick multilayer, the bonding energy difference between FTF and BTB pairs dominate the growth behavior during the molecular packing for thick layer growth.

CONCLUSIONS

Layer-by-layer growth of TiOPc is observed on the graphite surface, resulting from the asymmetric molecular shape and intrinsic dipole moment.[41,42,44,45] The deposition of TiOPc molecules onto the TiOPc MLs results in flat-lying MLs and thin multilayers involving dispersed, single molecular islands or cluster formation, consistent with ML-by-ML growth. While on Ag(111), the formation of a uniformly oriented TiOPc face up ML was ascribed to Ag(111) being able to screen the large ML dipole, on HOPG the formation of a uniform ML can only be attributed to the $\pi-\pi$ stacking interaction as confirmed by DFT calculations. Conversely, in thick multilayers, substrate effects are screened; therefore, the greater interaction energy for FTF vs BTB TiOPc pairs results in a growth-mode transition to BL-by-BL. This growth transition to BL-by-BL occurs at greater thickness (over 15 ML) on HOPG than on Ag(111),[43] consistent with the difference in screening of the TiOPc dipoles by Ag(111). As a result of the ML-by-ML and BL-by-BL growth modes, the deposited TiOPc films (10 nm) on the graphite surfaces are nearly homogeneous, crystalline, and molecularly flat, as shown in STM and AFM images. This growth mode results in the spontaneous deposition of molecularly flat films with large domain size on graphite surfaces without complicated seeding techniques. The results presented here demonstrate the impact of asymmetric charge density and shape of organic molecules on the growth behavior of films. Therefore, this model growth behavior of TiOPc opens the development of platform layers for organic transistors, OLEDs, and photovoltaic cells, and it can be applied to other weak interactive surfaces.

ASSOCIATED CONTENT

Supporting Information

The Supporting Information is available free of charge on the ACS Publications website at DOI: 10.1021/acs.jpcc.6b13096.

Experimental details, supporting STM and STS data of planar CuPc multilayers, and large area STM and AFM images of TiOPc films (PDF)

AUTHOR INFORMATION

Corresponding Author

*E-mail: akummel@ucsd.edu.

ORCID

Jun Hong Park: 0000-0001-5138-1622
Susan K. Fullerton-Shirey: 0000-0003-2720-0400
Pabitra Choudhury: 0000-0002-5023-9154

Notes

The authors declare no competing financial interest.

ACKNOWLEDGMENTS

The authors thank Dr. Darren Lipomi and Dr. Randall Feenstra for discussions about observed growth behavior of TiOPc and STS analysis. This work is supported by NSF Grant DMR 1207213 and by LEAST-STARnet, a Semiconductor Research Corporation program, sponsored by MARCO and DARPA and by SRC NRI SWAN.

REFERENCES

(1) Oosterhout, S. D.; Wienk, M. M.; van Bavel, S. S.; Thiedmann, R.; Koster, L. J. A.; Gilot, J.; Loos, J.; Schmidt, V.; Janssen, R. A. J. The Effect of Three-Dimensional Morphology on the Efficiency of Hybrid Polymer Solar Cells. *Nat. Mater.* **2009**, *8*, 818–824.

(2) Placencia, D.; Wang, W. N.; Gantz, J.; Jenkins, J. L.; Armstrong, N. R. Highly Photoactive Titanyl Phthalocyanine Polymorphs as Textured Donor Layers in Organic Solar Cells. *J. Phys. Chem. C* **2011**, *115*, 18873–18884.

(3) Tress, W.; Leo, K.; Riede, M. Dominating Recombination Mechanisms in Organic Solar Cells Based on Znpc and C-60. *Appl. Phys. Lett.* **2013**, *102* (16), 163901.

(4) Shah, S.; Biswas, R. Atomic Pathways Underlying Light-Induced Changes in Organic Solar Cell Materials. *J. Phys. Chem. C* **2015**, *119*, 20265–20271.

(5) Someya, T.; Sekitani, T.; Iba, S.; Kato, Y.; Kawaguchi, H.; Sakurai, T. A Large-Area Flexible Pressure Sensor Matrix with Organic Field-Effect Transistors for Artificial Skin Applications. *Proc. Natl. Acad. Sci. U. S. A.* **2004**, *101*, 9966–9970.

(6) Manunza, I.; Bonfiglio, A. Pressure Sensing Using a Completely Flexible Organic Transistor. *Biosens. Bioelectron.* **2007**, *22*, 2775–2779.

(7) Sokolov, A. N.; Tee, B. C. K.; Bettinger, C. J.; Tok, J. B. H.; Bao, Z. N. Chemical and Engineering Approaches to Enable Organic Field-Effect Transistors for Electronic Skin Applications. *Acc. Chem. Res.* **2012**, *45*, 361–371.

(8) Ren, X. C.; Chan, P. K. L.; Lu, J. B.; Huang, B. L.; Leung, D. C. W. High Dynamic Range Organic Temperature Sensor. *Adv. Mater.* **2013**, *25*, 1291–1295.

(9) Dinelli, F.; Murgia, M.; Levy, P.; Cavallini, M.; Biscarini, F.; de Leeuw, D. M. Spatially Correlated Charge Transport in Organic Thin Film Transistors. *Phys. Rev. Lett.* **2004**, *92* (11), 116802.

(10) Wang, S.; Kiersnowski, A.; Pisula, W.; Mullen, K. Microstructure Evolution and Device Performance in Solution-Processed Polymeric Field-Effect Transistors: The Key Role of the First Monolayer. *J. Am. Chem. Soc.* **2012**, *134*, 4015–4018.

(11) Takeya, J.; Yamagishi, M.; Tominari, Y.; Hirahara, R.; Nakazawa, Y.; Nishikawa, T.; Kawase, T.; Shimoda, T.; Ogawa, S. Very High-Mobility Organic Single-Crystal Transistors with in-Crystal Conduction Channels. *Appl. Phys. Lett.* **2007**, *90* (10), 102120.

(12) Briseno, A. L.; Mannsfeld, S. C. B.; Ling, M. M.; Liu, S. H.; Tseng, R. J.; Reese, C.; Roberts, M. E.; Yang, Y.; Wudl, F.; Bao, Z. N. Patterning Organic Single-Crystal Transistor Arrays. *Nature* **2006**, *444*, 913–917.

(13) Lunt, R. R.; Benziger, J. B.; Forrest, S. R. Relationship between Crystalline Order and Exciton Diffusion Length in Molecular Organic Semiconductors. *Adv. Mater.* **2010**, *22*, 1233–1236.

(14) Noriega, R.; Rivnay, J.; Vandewal, K.; Koch, F. P. V.; Stingelin, N.; Smith, P.; Toney, M. F.; Salleo, A. A General Relationship between Disorder, Aggregation and Charge Transport in Conjugated Polymers. *Nat. Mater.* **2013**, *12*, 1038–1043.

(15) De Arco, L. G.; Zhang, Y.; Schlenker, C. W.; Ryu, K.; Thompson, M. E.; Zhou, C. W. Continuous Highly Flexible and Transparent Graphene Films by Chemical Vapor Deposition for Organic Photovoltaics. *ACS Nano* **2010**, *4*, 2865–2873.

(16) Han, T. H.; Lee, Y.; Choi, M. R.; Woo, S. H.; Bae, S. H.; Hong, B. H.; Ahn, J. H.; Lee, T. W. Extremely Efficient Flexible Organic Light-Emitting Diodes with Modified Graphene Anode. *Nat. Photonics* **2012**, *6*, 105–110.

(17) Lee, G. H.; Lee, C. H.; van der Zande, A. M.; Han, M. Y.; Cui, X.; Arefe, G.; Nuckolls, C.; Heinz, T. F.; Hone, J.; Kim, P.

DOI: 10.1021/acs.jpcc.6b13096
J. Phys. Chem. C 2017, 121, 6721–6728

Heterostructures Based on Inorganic and Organic Van Der Waals Systems. *APL Mater.* **2014**, *2* (9), 092511.
(18) Wagner, S. R.; Lunt, R. R.; Zhang, P. P. Anisotropic Crystalline Organic Step-Flow Growth on Deactivated Si Surfaces. *Phys. Rev. Lett.* **2013**, *110* (8), 086107.
(19) Gustafsson, J. B.; Zhang, H. M.; Johansson, L. S. O. Stm Studies of Thin Ptcda Films on Ag/Si(111)-Root 3x Root 3. *Phys. Rev. B: Condens. Matter Mater. Phys.* **2007**, *75* (15), 155414.
(20) Cheng, Z. H.; Gao, L.; Deng, Z. T.; Liu, Q.; Jiang, N.; Lin, X.; He, X. B.; Du, S. X.; Gao, H. J. Epitaxial Growth of Iron Phthalocyanine at the Initial Stage on Au(111) Surface. *J. Phys. Chem. C* **2007**, *111*, 2656−2660.
(21) Wang, S. D.; Dong, X.; Lee, C. S.; Lee, S. T. Orderly Growth of Copper Phthalocyanine on Highly Oriented Pyrolytic Graphite (Hopg) at High Substrate Temperatures. *J. Phys. Chem. B* **2004**, *108*, 1529−1532.
(22) Kera, S.; Casu, M. B.; Bauchspiess, K. R.; Batchelor, D.; Schmidt, T.; Umbach, E. Growth Mode and Molecular Orientation of Phthalocyanine Molecules on Metal Single Crystal Substrates: A Nexafs and Xps Study. *Surf. Sci.* **2006**, *600*, 1077−1084.
(23) Xie, W. G.; Xu, J. B.; An, J.; Xue, K. Correlation between Molecular Packing and Surface Potential at Vanadyl Phthalocyanine/Hopg Interface. *J. Phys. Chem. C* **2010**, *114*, 19044−19047.
(24) Zhang, Y.; Diao, Y.; Lee, H.; Mirabito, T. J.; Johnson, R. W.; Puodziukynaite, E.; John, J.; Carter, K. R.; Emrick, T.; Mannsfeld, S. C. B.; et al. Intrinsic and Extrinsic Parameters for Controlling the Growth of Organic Single-Crystalline Nanopillars in Photovoltaics. *Nano Lett.* **2014**, *14*, 5547−5554.
(25) Gotzen, J.; Kafer, D.; Woll, C.; Witte, G. Growth and Structure of Pentacene Films on Graphite: Weak Adhesion as a Key for Epitaxial Film Growth. *Phys. Rev. B: Condens. Matter Mater. Phys.* **2010**, *81* (8), 085440.
(26) Gotzen, J.; Lukas, S.; Birkner, A.; Witte, G. Absence of Template Induced Ordering in Organic Multilayers: The Growth of Pentacene on a Cu(221) Vicinal Surface. *Surf. Sci.* **2011**, *605*, 577−581.
(27) Stohr, M.; Gabriel, M.; Moller, R. Investigation of the Growth of Ptcda on Cu(110): An Stm Study. *Surf. Sci.* **2002**, *507-510*, 330−334.
(28) Huang, H.; Chen, S.; Gao, X. Y.; Chen, W.; Wee, A. T. S. Structural and Electronic Properties of Ptcda Thin Films on Epitaxial Graphene. *ACS Nano* **2009**, *3*, 3431−3436.
(29) Su, M. S.; Kuo, C. Y.; Yuan, M. C.; Jeng, U. S.; Su, C. J.; Wei, K. H. Improving Device Efficiency of Polymer/Fullerene Bulk Heterojunction Solar Cells through Enhanced Crystallinity and Reduced Grain Boundaries Induced by Solvent Additives. *Adv. Mater.* **2011**, *23*, 3315−3319.
(30) Nie, W. Y.; Tsai, H. H.; Asadpour, R.; Blancon, J. C.; Neukirch, A. J.; Gupta, G.; Crochet, J. J.; Chhowalla, M.; Tretiak, S.; Alam, M. A.; et al. High-Efficiency Solution-Processed Perovskite Solar Cells with Millimeter-Scale Grains. *Science* **2015**, *347*, 522−525.
(31) Rosenow, T. C.; Walzer, K.; Leo, K. Near-Infrared Organic Light Emitting Diodes Based on Heavy Metal Phthalocyanines. *J. Appl. Phys.* **2008**, *103* (4), 043105.
(32) Hohnholz, D.; Steinbrecher, S.; Hanack, M. Applications of Phthalocyanines in Organic Light Emitting Devices. *J. Mol. Struct.* **2000**, *521*, 231−237.
(33) Wohrle, D.; Schnurpfeil, G.; Makarov, S. G.; Kazarin, A.; Suvorova, O. N. Practical Applications of Phthalocyanines - from Dyes and Pigments to Materials for Optical, Electronic and Photo-Electronic Devices. *Makrogeterotsikly* **2012**, *5*, 191−202.
(34) Williams, G.; Sutty, S.; Klenkler, R.; Aziz, H. Renewed Interest in Metal Phthalocyanine Donors for Small Molecule Organic Solar Cells. *Sol. Energy Mater. Sol. Cells* **2014**, *124*, 217−226.
(35) Marinelli, F.; Dell'Aquila, A.; Torsi, L.; Tey, J.; Suranna, G. P.; Mastrorilli, P.; Romanazzi, G.; Nobile, C. F.; Mhaisalkar, S. G.; Cioffi, N.; Palmisano, F. An Organic Field Effect Transistor as a Selective No(X) Sensor Operated at Room Temperature. *Sens. Actuators, B* **2009**, *140*, 445−450.
(36) Newton, M. I.; Starke, T. K. H.; Willis, M. R.; McHale, G. NO2 Detection at Room Temperature with Copper Phthalocyanine Thin Film Devices. *Sens. Actuators, B* **2000**, *67*, 307−311.
(37) Placencia, D.; Wang, W. N.; Shallcross, R. C.; Nebesny, K. W.; Brumbach, M.; Armstrong, N. R. Organic Photovoltaic Cells Based on Solvent-Annealed, Textured Titanyl Phthalocyanine/C-60 Heterojunctions. *Adv. Funct. Mater.* **2009**, *19*, 1913−1921.
(38) Tanaka, H.; Yasuda, T.; Fujita, K.; Tsutsui, T. Transparent Image Sensors Using an Organic Multilayer Photodiode. *Adv. Mater.* **2006**, *18*, 2230−2233.
(39) Hipps, K. W.; Barlow, D. E.; Mazur, U. Orbital Mediated Tunneling in Vanadyl Phthalocyanine Observed in Both Tunnel Diode and Stm Environments. *J. Phys. Chem. B* **2000**, *104*, 2444−2447.
(40) Gruenewald, M.; Peuker, J.; Meissner, M.; Sojka, F.; Forker, R.; Fritz, T. Impact of a Molecular Wetting Layer on the Structural and Optical Properties of Tin(Ii)-Phthalocyanine Multilayers on Ag(111). *Phys. Rev. B: Condens. Matter Mater. Phys.* **2016**, *93*, 115418.
(41) Kera, S.; Abduaini, A.; Aoki, M.; Okudaira, K. K.; Ueno, N.; Harada, Y.; Shirota, Y.; Tsuzuki, T. Characterization of Ultrathin Films of Titanyl Phthalocyanine on Graphite: Pies and Ups Study. *Thin Solid Films* **1998**, *327-329*, 278−282.
(42) Norton, J. E.; Bredas, J. L. Theoretical Characterization of Titanyl Phthalocyanine as a P-Type Organic Semiconductor: Short Intermolecular Pi-Pi Interactions Yield Large Electronic Couplings and Hole Transport Bandwidths. *J. Chem. Phys.* **2008**, *128* (3), 034701.
(43) Kröger, I.; Stadtmüller, B.; Kumpf, C. Submonolayer and Multilayer Growth of Titaniumoxide-Phthalocyanine on Ag(111). *New J. Phys.* **2016**, *18*, 113022.
(44) Kera, S.; Yabuuchi, Y.; Yamane, H.; Setoyama, H.; Okudaira, K. K.; Kahn, A.; Ueno, N. Impact of an Interface Dipole Layer on Molecular Level Alignment at an Organic-Conductor Interface Studied by Ultraviolet Photoemission Spectroscopy. *Phys. Rev. B: Condens. Matter Mater. Phys.* **2004**, *70* (8), 085304.
(45) Fukagawa, H.; Yamane, H.; Kera, S.; Okudaira, K. K.; Ueno, N. Experimental Estimation of the Electric Dipole Moment and Polarizability of Titanyl Phthalocyanine Using Ultraviolet Photoelectron Spectroscopy. *Phys. Rev. B: Condens. Matter Mater. Phys.* **2006**, *73*, 041302.
(46) Feenstra, R. M. Tunneling Spectroscopy of the (110)-Surface of Direct-Gap III-V Semiconductors. *Phys. Rev. B: Condens. Matter Mater. Phys.* **1994**, *50*, 4561−4570.
(47) Feenstra, R. M.; Lee, J. Y.; Kang, M. H.; Meyer, G.; Rieder, K. H. Band Gap of the Ge(111)C(2 × 8) Surface by Scanning Tunneling Spectroscopy. *Phys. Rev. B: Condens. Matter Mater. Phys.* **2006**, *73* (3), 035310.
(48) Bevington, P. R.; Robinson, D. K. *Data Reduction and Error Analysis for the Physical Sciences*, 3rd ed.; McGraw-Hill: Boston, MA, 2003; p xi.
(49) Guaino, P.; Carty, D.; Hughes, G.; McDonald, O.; Cafolla, A. A. Long-Range Order in a Multilayer Organic Film Templated by a Molecular-Induced Surface Reconstruction: Pentacene on Au(110). *Appl. Phys. Lett.* **2004**, *85*, 2777−2779.
(50) Ruiz, R.; Choudhary, D.; Nickel, B.; Toccoli, T.; Chang, K. C.; Mayer, A. C.; Clancy, P.; Blakely, J. M.; Headrick, R. L.; Iannotta, S.; et al. Pentacene Thin Film Growth. *Chem. Mater.* **2004**, *16*, 4497−4508.
(51) Braun, D.; Schirmeisen, A.; Fuchs, H. Molecular Growth and Sub-Molecular Resolution of a Thin Multilayer of Ptcda on Ag(110) Observed by Scanning Tunneling Microscopy. *Surf. Sci.* **2005**, *575*, 3−11.
(52) Choi, J.; Eom, C. B.; Rijnders, G.; Rogalla, H.; Blank, D. H. A. Growth Mode Transition from Layer by Layer to Step Flow During the Growth of Heteroepitaxial SrRuO3 on (001) SrTiO3. *Appl. Phys. Lett.* **2001**, *79*, 1447−1449.

DOI: 10.1021/acs.jpcc.6b13096
J. Phys. Chem. C 2017, 121, 6721−6728